Magnetic Resolver Using Hall-Effect Sensors

Ye Gu Kang
Electrical & Electronic Dept.
University of Oviedo
Gijón, Spain
email address or ORCID

Diego F. Laborda
Electrical & Electronic Dept.
University of Oviedo
Gijón, Spain
dflaborda@uniovi.es

Daniel Fernández
Electrical & Electronic Dept.
University of Oviedo
Gijón, Spain
fernandezalodaniel@uniovi.es

David Reigosa
Electrical & Electronic Dept
University of Oviedo
Gijon, Spain
diazdavid@uniovi.es

Fernando Briz
Electrical & Electronic Dept
University of Oviedo
Gijón, Spain
fernando@isa.uniovi.es

***Abstract*— Control of AC electric machines requires, in many cases, accurate knowledge of rotor position. Encoders and resolvers are the most widely used option in the industry. Variable reluctance (VR) resolvers are advantageous in harsh environments due to their robustness; however, they represent a significant portion of the total drive cost. This paper presents a magnetic resolver using low-cost Hall effect sensors. Advantages with conventional encoders include compactness and reduced cost, which are achieved without penalizing the other properties of VR resolvers. The proposed sensor is fully compatible with conventional drives and supports wide carrier frequency and supply voltage variations.**

Keywords—Magnetic Resolver, Hall-sensor, angular position measurement.

I. INTRODUCTION

Electric drives are used in a vast range of applications, including domestic, industrial, traction, aerospace, etc. Precise control of AC electric machines requires accurate knowledge of the rotor position. Optical encoders (optical-based angular position sensors) and resolvers (inductive-based angular position sensors), are the most used sensors in the industry [1]-[5], although many other alternatives have been reported in the literature: capacitive [2]-[3], inductive [4] or magnetic-based angular position sensors are available. Capacitive-based angular position sensors in [3], [4] provide high precision output but requires additional circuitry to be compatible with standard encoder or resolver signals. Inductive position sensors are axially planar [4], low weight, with a similar operation principle to a transformer but lack robustness. Magnetic angular position sensors are mainly based on Hall-effect or Giant Magnetoresistance (GMR) devices [16],[17]. Magnetic sensors used for automotive applications (e.g. throttle position detection, shaft position…) are also commercially available [16], [17]. The main drawbacks of these devices are the robustness decrease, inertia increase, and extra room. In addition, their accuracy depends on the offset or misalignment of the permanent magnet material that must be attached to the rotating part.

Optical encoders are likely the preferred option in general purpose applications and can provide incremental or, at a higher cost, absolute angular position. However, they often suffer from a limited range of temperature of operation and a reduced capability to withstand shock and vibration compared to resolvers.

This work was supported in part by the Research, Technological Development and Innovation Programs of the Spanish Ministry Economy and Competitiveness, under grant MINECO-17-ENE2016-80047-R and by the Government of Asturias under project IDI/2018/000188 and FEDER funds.

Resolvers inherently detect the absolute position and exhibit high vibration and shock withstand capability, a wide range of temperature of operation, and high rotational speed. Resolvers can be brushless [8], brushed (in disuse), or variable reluctance (VR) [9]-[10]. A brushless resolver is a rotatory transformer excited by AC voltage to the rotor winding [8]. An AC voltage is induced in the output winding (stator), which is modulated by the rotor position. VR resolvers do not have rotor windings and bearings and have both the output and the excitation windings in the stator; no brushes or rotating transformer is therefore required. They can be easily made frameless mounted, integrated into the motor without the need of a coupling device, and without adding friction to the system [7], what makes them appealing in traction applications (i.e. electric vehicles and hybrid electric vehicles), [7], [8]. Their main drawback, however, is the cost [6],[11].

This paper proposes an alternative design of a magnetic resolver using field sensors (i.e. Hall-effect) and a magnetized moving part made of non-laminated electrical steel and permanent magnets. Compared to VR resolver, the proposed design is simpler, more compact, cheaper, and easier manufacturability: it does not require stator/rotor laminations nor windings. Its power consumption is very low, and it can provide more than one independent output for a redundant mode of operation. It can be easily scalable in size, or the number of poles to meet the requirements of a specific application. Still, it will retain the main properties of VR resolver, and is fully compatible, meaning that no modification in the cabling or electronics of the drive is required.

The paper is organized as follows: principles of operation are discussed in Section II, design optimization is discussed in section III, and the validation of the model using FEA is presented in Section IV. Section V shows an assembly of the proposed prototype, and experimental results and conclusions are presented in sections VI and VII, respectively.

II. PRINCIPLE OF OPERATION OF OPERATION

A brief description of conventional resolvers aimed to establish the basis for the assessment of the proposed concept is presented following.

Resolvers can be classified into brushless wound field (WF) and variable reluctance (VR). Both are a special type

of rotary transformer that couples a primary winding (*Excitation* see Fig. 1) with two secondary windings (*Output 1 & 2*) that are 90 electrical degrees phase shifted. Excitation signal, i.e. $v_E(t)$ in Fig. 1, is generally a sine wave (1) (see Fig. 2a), of magnitude and angular frequency E_0 and ω_s, respectively. The output signals of the resolver are $v_S(t)$ **Error! Reference source not found.** and $v_C(t)$ **Error! Reference source not found.** (see Figs. 2b and 2c), where k is the equivalent turns ratio of the magnetic coupling, θ_r is the rotor position, X is a multiplication factor for the angle **Error! Reference source not found.**.

$$v_E(t) = E_0 \sin(\omega_s t) \tag{1}$$

$$v_S(t) = E_0 \sin(\omega_s t) k \sin(X\theta_r) \tag{2}$$

$$v_C(t) = E_0 \sin(\omega_s t) k \cos(X\theta_r) \tag{3}$$

$$v_S'(t) = k \sin(X\theta_r) \tag{4}$$

$$v_C'(t) = k \cos(X\theta_r) \tag{5}$$

Voltages $v_S(t)$ and $v_C(t)$ are the input to a resolver-to-digital (R/D) converter, which typically includes a demodulation stage to subtract the excitation signal; **Error! Reference source not found.** and **Error! Reference source not found.** being obtained after the demodulation. A large variety of methods have been reported to obtain the rotor position, θ_r, from **Error! Reference source not found.** and **Error! Reference source not found.** [15].

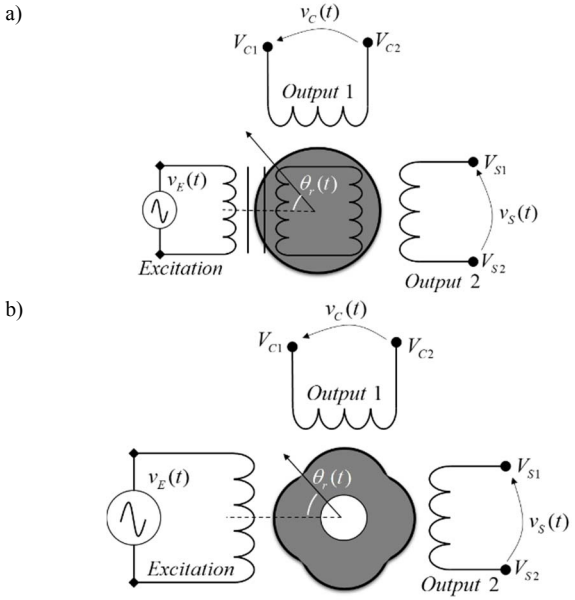

Fig. 1. Resolvers, a) WF and b) VR.

Rotor winding of WF resolvers is excited by an AC voltage, which can be produced by means of a magnetic coupling (i.e. brushless WF, see Fig. 1a). Voltages in the stator windings are a *sine* and *cosine* signal, which is modulated by the rotor angle θ_r. In VR resolvers, excitation winding is also placed in the stator (see Fig. 1b), avoiding the use of brushes or slip rings. In addition, they can be in-shaft installed. An AC voltage/current signal is injected into the excitation winding, the resulting voltages in the two stator windings being a *sine* and *cosine* signals whose angle is modulated by the rotor angle as for the WF case. VR resolvers have a wider temperature range of operation and, with simple and robust construction, are less sensitive to noise and allow longer transmission cables Error! Reference source not found. ,Error! Reference source not found..

A. Principle of Operation of the proposed magnetic resolver

The proposed magnetic resolver is schematically shown in Fig.3. It consists of a rotor and a stator: the rotor is made of a non-laminated ferromagnetic core and permanent magnets (*PMs* in Fig.3); the stator consists of two Hall-effect sensors 90 electrical degrees phase shifted. Linear Hall-effect integrated circuit (IC) sensors will be used for the assembly of the proposed magnetic resolver. These types of ICs allow current control through the Hall element without integrated electronics.

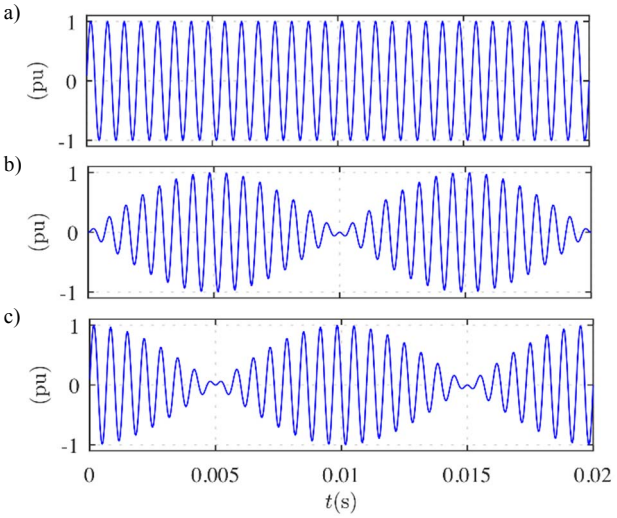

Fig. 2. Resolver signals, a) *excitation*, $v_e(t)$, b) *Output 1* of the resolver, $v_c(t)$ (i.e. *cosine*), c) *Output 2* of the resolver, $v_s(t)$ (i.e. *sine*). $\omega_s = 2 \cdot \pi \cdot 500$ rad/s, $\omega_r = 2 \cdot \pi \cdot 50$ rad/s

Hall-effect sensors are usually fed using DC voltage (6) or current, see Fig. 4a. The output voltage (Hall voltage) of the Hall-effect sensors $v_{HS}(t)$ and $v_{HC}(t)$ (see Fig. 3) for the case of a constant rotor speed are (7)-(8), (see Fig. 4b and Fig. 4c). While these signals are modulated by the rotor position, they differ from the signals provided by conventional resolvers, where the position information signals produce an amplitude modulation of a carrier signal (see Fig. 2). Alternatively, the Hall-effect sensors can be fed with and AC voltage (or current). The output voltages depending on the rotor speed will be in this case (11)-(12) (see Fig. 4d and Fig. 4f), which are equal to the signals provided by conventional resolvers. For every pair of poles (p) in the rotor, four Hall-effect sensors can be installed in the rotor providing duplicated signals for applications where redundancy is required.

It must be remarked that (11)-(12) results from a sinusoidal flux distribution in the rotor surface. Rotor design to achieve this target is described following.

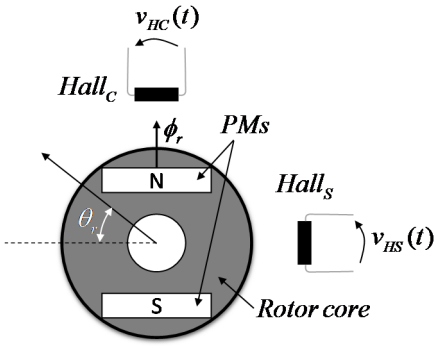

Fig. 3. Schematic representation of the proposed magnetic resolver and position of the Hall-effect sensors.

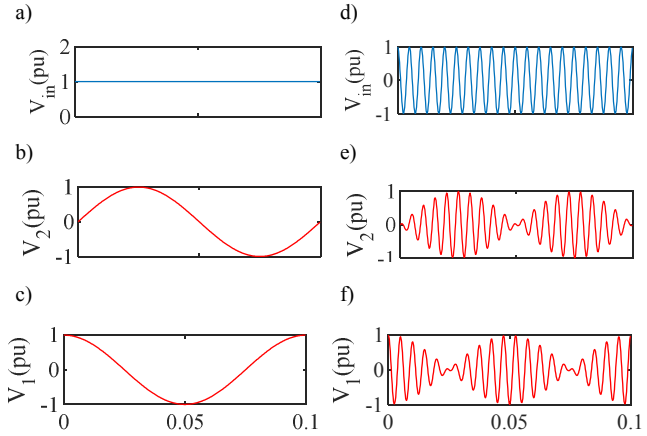

Fig. 4. Excitation and resulting waveforms of the proposed resolver: a) DC excitation, b) Sin output for DC excitation, c) Cos output for DC excitation, d) AC excitation, e) sin output for AC excitation and f) cos output for AC excitation.

$$v_E(t) = E_0 \tag{6}$$

$$v_{HS}(t) = k \sin(\theta_r) \tag{7}$$

$$v_{HC}(t) = k \cos(\theta_r) \tag{8}$$

$$v'_{Hall}(t) = k\, i(t) B(t) \tag{9}$$

$$v_E(t) = E_0 \sin(\omega_s t) \tag{10}$$

$$v_{HS}(t) = E_0 \sin(\omega_s t) k \sin(\theta_r) \tag{11}$$

$$v_{HC}(t) = E_0 \sin(\omega_s t) k \cos(\theta_r) \tag{12}$$

$$MO = Penalty + \sum_{n=1}^{3} O_n w_n \tag{13}$$

III. Rotor Design Optimization of the Proposed Magnetic Resolver

The optimization technique applied to the proposed magnetic resolver is explained in this section. The rotor geometry is evaluated to achieve three main targets: reduced use of magnetic materials, high fundamental flux amplitude and low harmonic distorsion on the flux density waveform.

Differential evolution optimization technique [13] was used to find the optimum solution in the design space using 2D finite element analysis (FEA). Rotor parameters are shown in Fig. 4 and Table. II.

The desired properties of the hall effect sensor based resolver are included in the objective function variable, O_n, in the multi-objective (MO) in (13): the magnitude of the airgap flux density, Q_2, Total harmonic distortion (THD) of the flux density, Q_1, and the volume of the permanent magnet (PM), Q_3. The fundamental component of the airgap flux density will decide the sensitivity of the proposed resolver, where the level of THD indicates the quality of the signal for the rotor position estimation. The PM volume is included in the objective function to result in a low-cost, high accuracy resolver. The goal for the multi-objective optimization is to find a minimum cost of the MO in (13), where w_n is the weighting factor of each objective variable. More details about the variable used in the multi-objective optimization is in Table I. The penalty is used for eliminating designs that violate the geometric constraints set for the geometrical parameters shown in Table II.

TABLE I. Parameters Of The Multy-Objective Function

Symbol	*Function*	*Definition*
O_1	THD	Harmonic distortion of flux in %
O_2	$(B_{Hall} - 0.08)^2$	Fundamental flux amplitude in Tesla with a target amplitude of 0.08
O_3	PM Volume	Magnet volume in mm^3
w_1	20	Weighting factor of O_1
w_2	20000	Weighting factor of O_2
w_3	10	Weighting factor of O_3
Penalty	0 if within the boundary 100 if outside boundary	Penalty is given when the input variables are outside the minimum and maximum range.

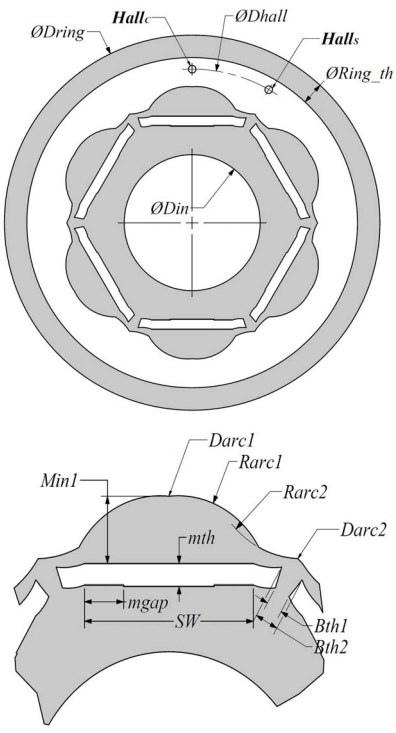

Fig. 4. Dimensions of the magnetic resolver a), general view and b), detailed view.

The resulting optimized resolver design, therefore, will be high sensitivity, low distortion, low-cost given the pre-defined boundary conditions. Three different types of

permanent magnet materials have been evaluated: Ferrite, sintered NdFeB, and bonded NdFeB magnets. Table III summarizes the optimization results.

TABLE II. GEOMETRIC PARAMETERS DESCRIPTION

Symbol	***Definition***
Darc1	Rotor d-axis outer diameter
Darc2	Rotor q-axis outer diameter
ϕDhall	Hall sensor distance from center
ϕDin	Rotor inner diameter
ϕDring	Ring outer diameter
Ring_th	Ring thickness
Rarc1	Rotor d-axis outer arc
Rarc2	Rotor q-axis outer arc
mth	Magnet thickness
Min1	Magnet distance from ϕDarc1
mgap	Magnet gap in slot
SW	Slot width
Bth1	Outer bridge thickness
Bth2	Inner bridge thickness

Fig. 5 shows an example of the flux distribution when using the selected geometry for the three permanent magnet materials, main properties of each case being shown in Table III. As expected, the maximum peak flux density in the airgap is obtained with the prototype equipped with sintered NdFeB magnets, see Table III. This will allow better use of the measuring range of the Hall-effect sensor, eventually improving the signal to noise ratio. Obtaining a similar peak flux density, bonded NdFeB magnets requires almost twice of magnetic material, see Table III. Ferrite magnets provide, as expected, the smallest flux density, with a peak value in around half of that obtained with NdFeB magnets. The Ferrite vs. NdFeB volume to achieve the same peak flux density is around 2.5, see Table III. Even in this case, the ferrite-based solution is expected to be cheaper.

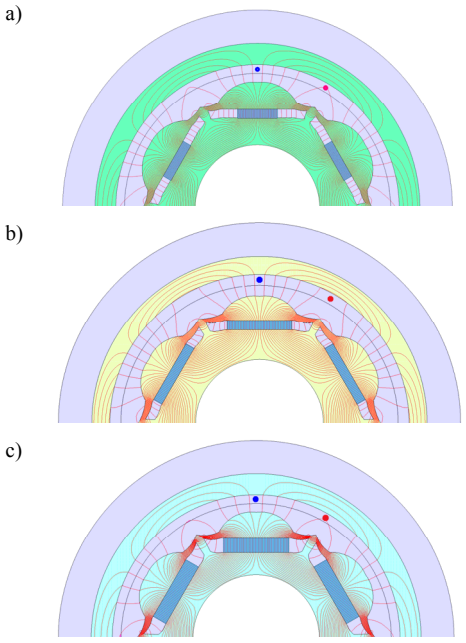

Fig. 5. Flux lines distribution for the optimized magnetic resolver design equipping a) Sintered NdFeB magnets, b) Bonden NdFeB magnets, and c) Ferrite magnets. Blue (•) and red (•) spots represent the $Hall_c$ and $Hall_s$ sensors.

TABLE III. OPTIMIZATION RESULTS OF THE MAGNETIC RESOLVER

	PM Material		
	Ferrite	***Sintered NdFeB***	***Bonded NdFeB***
THD (%)	*1.55*	*0.27*	*0.84*
Fundamental flux amplitude (mT)	*36.23*	*95.81*	*86.68*
PM volume (mm^3)	*97.33*	*37.16*	*60.65*

[a.] Results obtained from FEA simulation

IV. VALIDATION OF THE RESOLVER USING FEA

This section shows FEA results for the three optimized prototypes using sintered NdFeb, bonded NdFeB, and Ferrite, respectively.

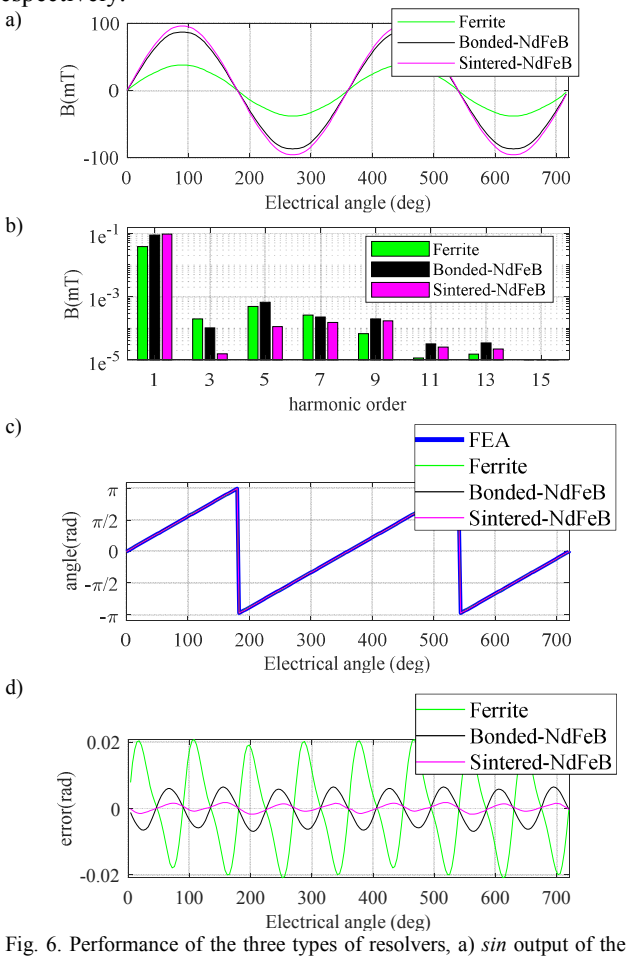

Fig. 6. Performance of the three types of resolvers, a) *sin* output of the hall effect sensors, b) FFT of *sin* output (in a)), c) resulting position angle and d) resulting angle error.

Fig. 6a shows the magnetic flux density at the position of "$Hall_s$" sensor (see Fig. 3 and 5) for one rotor revolution for the three cases. Fig. 6b shows the corresponding FFTs, from which the THDs in Table III are obtained. It can be observed that the THD in all cases is <1.55%, all harmonics being at least two orders of magnitude smaller than the fundamental component. It is noted that these results might be influenced by the bandwidth of the Hall-Effect sensors, which is typically >250kHz [12]; I.e., the bandwidth of the Hall-effect sensors will have virtually no influence in standard machines used in traction applications [14]. Fig. 6c shows the measured position for the three different rotor designs and the real position (i.e. FEA). Fig. 6d shows the error in the measured position, which is due to the harmonics in the flux waveform shown in Fig. 6b and does not account for errors due to assembling tolerances, circuitry, noise, misalignments, etc.

It can be observed in Fig. 6d that the lower error is obtained for the sintered NdFeB magnet, ferrite magnets showing the worst behavior. Measurement errors are ±1.1º (Ferrite based), ±0.35º (bonded NdFeB based), and ±0.09º (sintered NdFeB based). Position error of commercially available resolvers is in the range of ±0.5-1.0º for VR resolvers [11] and around ±0.16º for brushless resolvers, meaning that the accuracy is comparable with commercially available resolvers.

V. Assembly Of The Proposed Prototype

The proposed prototype can be assembled in two different configurations: in-shaft mounting and shaft-type for connections through flexible couplings. In any case, the necessary circuitry is the same, both allowing redundant configuration (i.e. providing duplicated signals). Fig. 7a shows the laser cutout of the optimized designs for the prototypes equipping Ferrite magnets and sintered NdFeB magnets, the PM samples being shown in Fig. 7b. The same laser cutout and magnets will be used for both the in-shaft and shaft-type resolvers.

a)

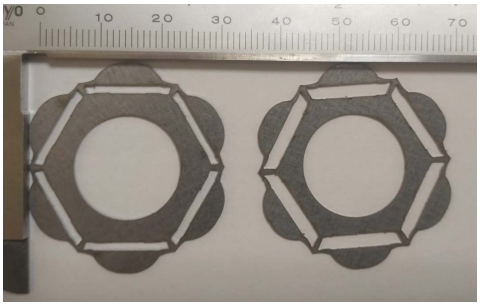

b)

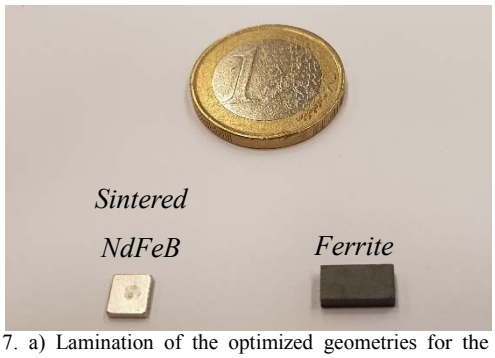

Fig. 7. a) Lamination of the optimized geometries for the magnetic resolver design equipping: sintered NdFeB (left) and Ferrite (right), Scale in mm, and b) NdFeB and Ferrite magnets for the designs in Fig. 7a.

A. Shaft-type assembly

The shaft-type magnetic resolver is shown in Fig. 8. It is equipped with the rotor cutout and PMs shown in Fig 7. It was designed with a Ø8 mm shaft, the diameter of the body and axial dimensions being Ø52 mm and 17 mm respectively. This design is suitable for the connection through flexible couplings. It can be observed that the PCB integrates four Hall-effect sensors (i.e. two $Hall_C$ and two $Hall_S$), i.e. it provides redundant output signals. The design also includes two bearings: front and rear cover hosts.

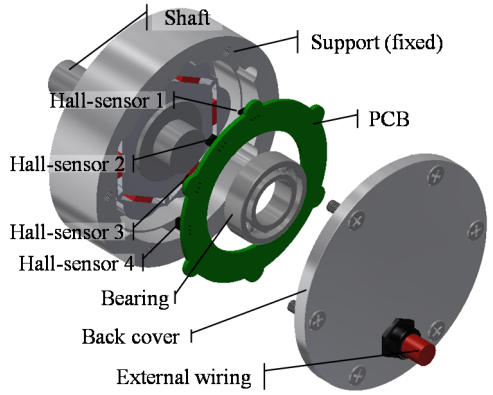

Fig. 8. Disassemble view of the Shaft-type magnetic resolver

B. In-shaft mount assembly

The in-shaft type magnetic resolver is shown in Fig. 9. It is equipped with the rotor cutout and PMs shown in Fig 7. The rotor of the sensor is directly connected to the machine shaft and fixed by a nut. The axial length of the sensor exploding bolts is 5 mm, and the diameter of the sensor is Ø 70 mm. In this case, the PCB integrates only two Hall-effect sensors (i.e. $Hall_C$ and $Hall_S$), although this design also allows redundant configuration. This design requires no bearings..

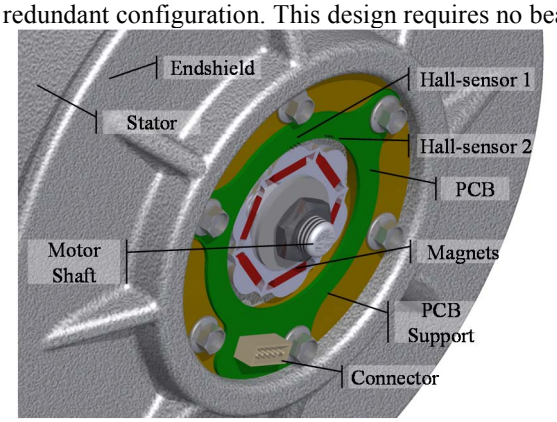

Fig.9 In-shaft type magnetic resolver inserted in an endshield of a machine.

C. Electronic circuitry

A conditioning system is required for the proposed prototype to achieve full compatibility with commercial drives in terms of power supply and output voltage levels. Its objective is twofold: provide supply voltages for the Hall elements and the additional ICs, and adapt output voltage levels within the range of commercial drives.

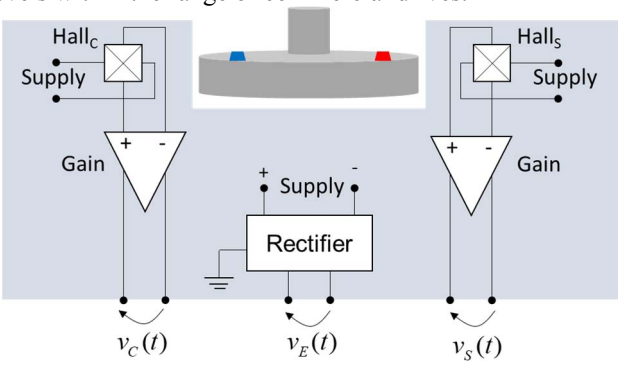

Fig. 10. Simplified representation of the electronic circuitry.

Fig. 8 shows a simplified representation of the electronic circuit needed for the proposed sensor. The excitation signal,

which will be provided by the drive (i.e. standard resolver excitation), is rectified to provide symmetrical voltage supply to the circuit, as demanded by the operational amplifiers. Hall elements (i.e. $Hall_C$ and $Hall_S$) are feed using constant voltage what produces a constant current through the hall elements since hall elements are resistors from an electrical point of view. Note that a temperature variation of the hall element will have a direct impact on the current through the hall element. However, this will not affect the position measurement since the rotor position information is included the phase of the current waveforms but not in the amplitude (see Fig. 2).

The total power consumption of the proposed system is in the range of the power consumption of the Hall-elements: 12.5 mW per sensor. The power consumption of the rectification stage can be negligible (i.e., conduction losses of a rectifier diode). The power consumption of the gain stages can also be negligible since ultra-low power differential operational amplifiers are used.

The circuit in Fig. 8 provides differential output signals to enhance noise immunity in the transmission wire.

VI. Experimental Results

A prototype of the shaft-type sensor is shown in Fig. 11, corresponding to the drawing in Fig.8. In this design, the fixed parts of the sensor (i.e. shaft, stator and cover) have been 3D printed using polyacid material (PLA). The moving parts (i.e., magnets and rotor) are made of Sintered NdFeB magnets and the laser-cut silicon steel 50H350, see Fig. 7. The prototype integrates two pairs of Hall-effect sensors (i.e. $Hall_C$ and $Hall_S$) for a redundant output, the simplified power and conditioning stages for each pair of sensors being shown in Fig. 10.

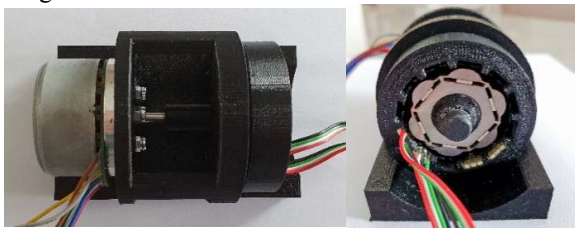

Fig.11. 3D printed position sensor (rigth) and testbench (left)

The sensor is attached to a brushless PMS motor in a testbench, see Fig. 11. Fig. 12 shows the output waveforms provided by a pair of Hall-effect sensors (i.e. $Hall_C$ and $Hall_S$) when they are fed with a sinusoidal waveform of $7V_{RMS}$ at 10 kHz. It can be observed that the peak amplitude of the magnetic flux density waveform in Fig. 13 is around 100mT, what matches the optimization results in Table III for sintered NdFeB magnets.

Fig. 12 shows the simplified signal processing used for speed and position estimation. Measured flux densities by $Hall_C$ and $Hall_S$ are multiplied by the excitation signal at the demodulation stage. The phase of the resulting complex vector signals, V_α ,V_β are normalized (14) and $\vec{V}_{dq}^{\,r}$ (15)-(16), is obtained using a synchronous reference frame phase-locked loop (SRF-PLL), which provides the estimated rotor speed and position [18].

The signal processing scheme in Fig. 12 is applied to the signals in Fig.13. Rotot speed and position are obtained from the waveforms in Fig.13 after the demodulation process, that are later normalized in amplitude (see Fig. 14) in order to feed a the SFR-PLL in Fig. 12.

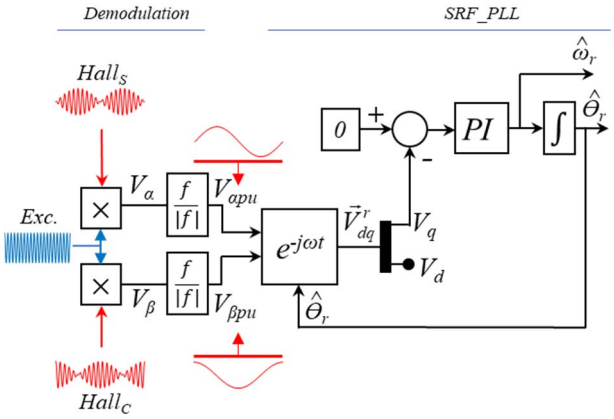

Fig.12 Schematic representation of the signal processing used for speed and position estimation

$$V_{\alpha pu} = \frac{V_\alpha}{|V_\alpha|}; \quad V_{\alpha pu} = \frac{V_\alpha}{|V_\alpha|} \tag{14}$$

$$\vec{V}_{\alpha\beta pu}^{\,s} = V_{\alpha pu} + jV_{\beta pu} \tag{15}$$

$$\vec{V}_{dq}^{\,r} = \vec{V}_{\alpha\beta pu}^{\,s} e^{-j\theta_r} \tag{16}$$

Fig. 15 shows the estimated speed obtained from the proposed sensor during the startup of the brushless machine in open loop. The machine is stopped until 2.75 s, and at t=2.75s the speed increases up to 20 rad/s. Fig. 16 shows the estimated absolute angular position. An aluminum design of the system with more accurate tolerances and higher stiffness is currently under development.

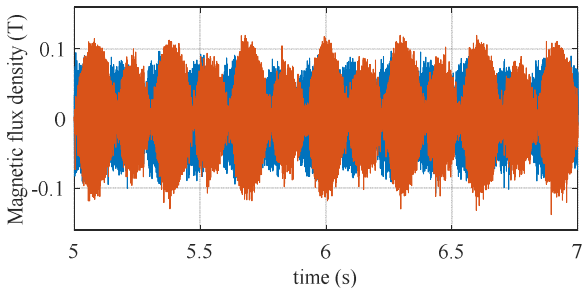

Fig. 13. Magnetic resolver signals: Hallc signal (blue), Vc(t) (i.e. cosine) amd Halls signal (red), Vs(t) (i.e. sine). ωs = 2· π · 10000 rad/s, ωr = 2· π · 1.1 rad/s

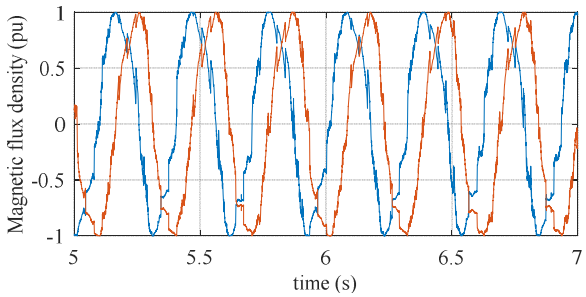

Fig. 14. Normalized magnetic resolver signals: Hallc signal (blue), Vc(t) (i.e. cosine) and Halls signal (red), Vs(t) (i.e. sine) ωs = 2· π · 10000 rad/s, ωr = 2· π · 1.1 rad/s

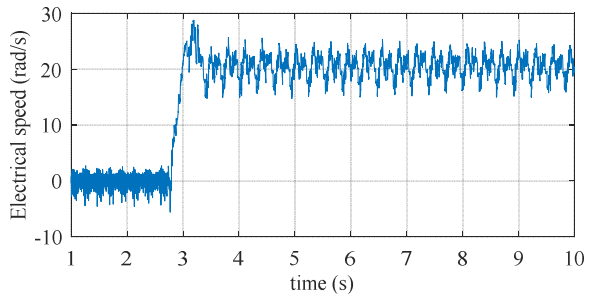

Fig. 15. Speed profile obtained with the proposed sensor. ωs = 2· π · 10000 rad/s, ωr = 2· π · 1.1 rad/s

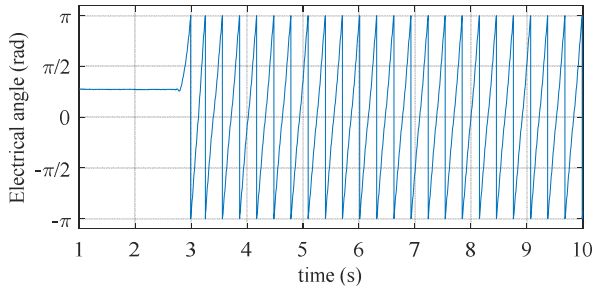

Fig. 16. Angular position profile obtained with the proposed sensor. ωs = 2· π · 10000 rad/s, ωr = 2· π · 1.1 rad/s

VII. Conclusions

A magnetic resolver using hall effect sensors is proposed in this paper. Compared to available resolvers, it provides similar accuracy, with a simpler and cheaper construction. Two different designs have been proposed: shaft-type or in-shat designs; both allowing redundant position measurement. FEA results have been provided to demonstrate the viability of the proposed system and the system has been experimentally validated.

Acknowledgment

Author would like to thank Bomatec AG for advising and providing magnet samples.

References

[1] R. M. Kennel, "Why Do Incremental Encoders Do a Reasonably Good Job in Electrical Drives with Digital Control?," Conference Record of the 2006 IEEE Industry Applications Conference Forty-First IAS Annual Meeting, Tampa, FL, 2006, pp. 925-930.doi: 10.1109/IAS.2006.256635

[2] B. Hou, C. Li, Z. Gao, Q. Wei, B. Zhou and R. Zhang, "Design, Optimization, and Compensation of a High-Precision Single-Excitation Absolute Capacitance Angular Encoder up to ±4’’," in IEEE Transactions on Industrial Electronics, vol. 66, no. 10, pp. 8161-8171, Oct. 2019. doi: 10.1109/TIE.2018.2886762

[3] [3]. H. Pu, H. Wang, X. Liu, Z. Yu and K. Peng, "A High-Precision Absolute Angular Position Sensor With Vernier Capacitive Arrays Based on Time Grating," in IEEE Sensors Journal, vol. 19, no. 19, pp. 8626-8634, 1 Oct.1, 2019. doi: 10.1109/JSEN.2019.2921479

[4] M. Howard, Incremental encoders, absolute encoders & pseudo-absolute encoders, Feb. 2013. Accessed on: Dec. 15, 2019. [Online]. Available: https://www.zettlex.com/wp-content/uploads/2017/08/incremental-encoders-vs.-absolute-encoders_Rev_3.1.pdf

[5] F. Jiang, D. Lou, H. Zhang, L. Tang, S. Sun and K. Yang, "Design of a GMR-based magnetic encoder using TLE5012B," 2017 20th International Conference on Electrical Machines and Systems (ICEMS), Sydney, NSW, 2017, pp. 1-4. doi: 10.1109/ICEMS.2017.8056197

[6] C. Jin, I. Jang, J. Bae, J. Lee and W. Kim, "Proposal of Improved Winding Method for VR Resolver," in IEEE Transactions on Magnetics, vol. 51, no. 3, pp. 1-4, March 2015, Art no. 8102404. doi: 10.1109/TMAG.2014.2348321

[7] L. Sun, "Analysis and Improvement on the Structure of Variable Reluctance Resolvers," in IEEE Transactions on Magnetics, vol. 44, no. 8, pp. 2002-2008, Aug. 2008. doi: 10.1109/TMAG.2008.923315

[8] J. Figueiredo, “Resolver models for manufacturing,” IEEE Trans. Ind. Electron., 58(8): 3693–3700, Aug. 2011.

[9] L. Z. Sun, J. B. Zou, and Y. P. Lu, “New variable-reluctance resolver for rotor-position sensing,” in Proc. IEEE Region 10th Conf. TENCON, vol. 4. Chiang Mai, Thailand, pp. 5–8, Nov. 2004.

[10] H. Saneie, Z. Nasiri-Gheidari and F. Tootoonchian, "Design-Oriented Modelling of Axial-Flux Variable-Reluctance Resolver Based on Magnetic Equivalent Circuits and Schwarz–Christoffel Mapping," in IEEE Transactions on Industrial Electronics, vol. 65, no. 5, pp. 4322-4330, May 2018, doi: 10.1109/TIE.2017.2760862.

[11] T. Suzuki, K. Toyotake and Y. Yamashita. “Variable reluctance type resolver rotor and brushless motor.” Japan Patent JP2010048775A, Aug. 25, 2008.

[12] D. Fernandez et al., "Permanent Magnet Temperature Estimation in PM Synchronous Motors Using Low-Cost Hall Effect Sensors," in IEEE Transactions on Industry Applications, vol. 53, no. 5, pp. 4515-4525, Sept.-Oct. 2017. doi: 10.1109/TIA.2017.2705580

[13] S. Das and P. N. Suganthan, "Differential Evolution: A Survey of the State-of-the-Art," in IEEE Transactions on Evolutionary Computation, vol. 15, no. 1, pp. 4-31, Feb. 2011. doi: 10.1109/TEVC.2010.2059031

[14] M. Minowa, H. Hijikata, K. Akatsu and T. Kato, "Variable leakage flux interior permanent magnet synchronous machine for improving efficiency on duty cycle," 2014 International Power Electronics Conference (IPEC-Hiroshima 2014 - ECCE ASIA), Hiroshima, 2014, pp. 3828-3833. doi: 10.1109/IPEC.2014.6870049

[15] L. Pecly, R. Schindeler, D. Cleveland and K. Hashtrudi-Zaad, "High-Precision Resolver-to-Velocity Converter," in IEEE Transactions on Instrumentation and Measurement, vol. 66, no. 11, pp. 2917-2928, Nov. 2017.doi: 10.1109/TIM.2017.2714378

[16] P. Kejik, S. Reymond and R. S. Popovic, "Circular Hall Transducer for Angular Position Sensing," TRANSDUCERS 2007 - 2007 International Solid-State Sensors, Actuators and Microsystems Conference, Lyon, 2007, pp. 2593-2596. doi: 10.1109/SENSOR.2007.4300702

[17] K. Bienczyk, "Angle measurement using a miniature hall effect position sensor," 2009 2nd International Students Conference on Electrodynamic and Mechatronics, Silesia, 2009, pp. 21-22. doi: 10.1109/ISCON.2009.5156096

[18] D. Reigosa, D. Fernandez, C. González, S. B. Lee and F. Briz, "Permanent Magnet Synchronous Machine Drive Control Using Analog Hall-Effect Sensors," in IEEE Transactions on Industry Applications, vol. 54, no. 3, pp. 2358-2369, May-June 2018, doi: 10.1109/TIA.2018.2802950.